VIP **Lithography**

A Route to Three-Dimensional Structures in a Microfluidic Device: Stop-Flow Interference Lithography**

Ji-Hyun Jang, Dhananjay Dendukuri, T. Alan Hatton, Edwin L. Thomas, and Patrick S. Doyle*

Polymeric structures with repeating 2D and 3D motifs at the micrometer scale and below have a variety of uses. Patterned 2D structures have been shown to have myriad applications in biosensors,[1] tissue engineering,[2] and diagnostic assay systems.[3] The availability of more sophisticated 3D structures would enable important advances in photonics,[4] information storage,[5] and tissue engineering.[6,7] Many techniques have been developed to fabricate complex 3D structures at the micrometer scale and below using either top-down or bottom-up approaches. Bottom-up approaches such as polymer phase separation,[8] molecular self-assembly,[9] or colloidal assembly[10] are cheap and can cover large areas but face defects and limitations in the type and the geometry of structures that can be formed. While top-down methods offer precise size and shape control, the necessary point-by-point or layer-by-layer processing makes methods such as gray-scale photolithography,[11] direct 3D writing,[12] or two-photon lithography[13] very time-consuming.

Recently, interference lithography (IL)[14–20] has emerged as an attractive alternative technique that allows the rational design of complex and defect-free 1D, 2D, and 3D patterns over large areas. Besides being fast and efficient, IL also affords control over geometrical parameters, such as symmetry and volume fractions, of the structures formed. IL performed using an elastomeric poly(dimethylsiloxane) (PDMS) phase mask[17] has the further advantage of providing simple and cheap processing, since only a single collimated beam is needed to form 3D interference patterns. However, phase-mask interference lithography (PMIL)[15,17] is typically

performed by flood exposing a spin-coated layer of photoresist film through a phase mask, thus imposing some restrictions on the shape and material properties of the structures formed as well as limiting the throughput because of the serial nature of processing. Furthermore, such processes are not easily amenable to the fabrication of chemically anisotropic structures. Chemical anisotropy refers to the presence of multiple segregated chemical functionalities or gradients of one or more chemical functionality in a structure. The synthesis of structures with controllable material properties and texturing across multiple length scales is important for a variety of applications, such as tissue engineering,[2] self-assembly,[21] and particle diagnostics.[3] To address this challenge, several microfluidic techniques that combine traditional photopolymerization or lithography with the unique properties of flow at the micrometer scale have emerged recently.[22,23] Doyle and co-workers developed a simple, flow-through microfluidic process called stop-flow lithography (SFL)[24] that enables photolithography to be performed in a flowing stream of oligomer. This setup enables the high-throughput synthesis of large numbers of micrometer-sized particles in any 2D extruded shape using a variety of polymer precursors.[24] The method also provides the ability to finely and conveniently tune the chemical anisotropy of the structures formed. However, the use of transparency masks has, to date, restricted this method to the formation of solid 2D shapes with relatively large feature sizes.[22,25]

Herein, we report a novel microfluidic stop-flow interference lithography (SFIL) technique that integrates the complementary aspects of PMIL with SFL. SFIL enables the high-throughput synthesis of three-dimensionally patterned, transparency-mask-defined polymeric particles with sub-micrometer feature sizes using liquid, biocompatible, oligomeric precursors. Advantages in throughput result from the ability to repeatedly form and flush out arrays of structured particles in under a second. This speed stems from the oxygen-induced inhibition[26] of free-radical polymerization reactions at PDMS surfaces, as explained in earlier work.[22] Material advantages result from the fact that even freely flowing oligomer liquids of low viscosity can be patterned in a continuous fashion without the requirement that they be spin-coated, exposed, and developed in a step-by-step fashion. The properties of the structures formed can be finely tuned by varying light intensity as well as photoinitiator and inhibitor concentrations. Chemical anisotropy can be introduced by exploiting the laminar co-flow of liquids in a microfluidic device, which results from the dominance of diffusive over convective transport.[27] The formation of such anisotropic, patterned structures using SFIL is shown. Finally, the utility of

[*] Dr. J.-H. Jang,[+] Prof. E. L. Thomas
Institute for Soldier Nanotechnologies
Department of Materials Science and Engineering
Massachusetts Institute of Technology
Cambridge, MA 02139 (USA)
Fax: (+1) 617-252-1175
E-mail: elt@mit.edu

Dr. D. Dendukuri,[+] Prof. T. A. Hatton, Prof. P. S. Doyle
Institute for Soldier Nanotechnologies
Department of Chemical Engineering
Massachusetts Institute of Technology
Cambridge, MA 02139 (USA)
Fax: (+1) 617-324-0066
E-mail: pdoyle@mit.edu

[+] These authors contributed equally to this work.

Take advantage of blue reference links

the patterned particles in increasing the sensitivity of particle-based biosensors is demonstrated.

A schematic diagram of the setup used for SFIL is shown in Figure 1. The microfluidic device and the phase mask, both molded in PDMS, are sealed to each other as shown in the cross-sectional view in Figure 1 a. When collimated light passes through the phase mask, a complex 3D distribution of light intensity is generated. This distribution induces cross-linking of the oligomer only in the high-intensity regions, thus leading to the formation of a 3D structure. A protective, 3-μm-thick PDMS layer is laminated on top of the phase mask to prevent the liquid oligomer from filling up the interstitial spaces that provide the refractive index difference that is required when light traverses through the phase mask. We used microfluidic devices with a lateral dimension of 1–5 mm to synthesize both millimeter-sized structures as well as arrays of micrometer-sized particles. The integrated device is placed on a microscope stage, and collimated light is provided either by a laser or by unfocused UV light from a Hg lamp that passes through a blackened, hollow metal tube. A mask corresponding to the shape of the desired structure is placed in the field stop of the microscope or in the path of the laser. Liquid poly(ethylene glycol) diacrylate (PEGDA) oligomer containing photoinitiator flows through the microfluidic device, as described in the Experimental Section. Poly(ethylene glycol)-based (PEG-based) hydrogel polymers, which minimize nonspecific binding, are well-suited for use in biological applications. We illustrate the method by forming PEGDA equilateral triangular prisms with a side length of 60 μm and a thickness of 25 μm using a phase mask that has a square, 2-μm periodic surface pattern. The particles are formed in a stationary layer of oligomer film using an exposure time of 300 ms and then flushed out into a reservoir. Differential interference contrast (DIC) images of the structures right after they are formed in the channel are shown in Figure 1 b. In Figure 1 c, we show DIC images of the particles from Figure 1 b after they have been suspended in ethanol. The phase-mask-induced pattern is clearly visible in the close-up DIC and SEM images of the triangular particles shown in the inset of Figure 1 c. These monodisperse, 60-μm particles were synthesized at a rate of 10 000 per hour.

SEM images of the typical structures formed by SFIL are shown in Figure 2. An image of the microfluidic device integrated with the phase mask and of the phase mask (inset) are shown in Figure 2 a. To minimize an inherent DC offset of the light intensity and to better control the propagation of radical transfer, we added a small amount of radical inhibitor (hydroquinone).[28] By controlling light intensity and inhibitor concentration, structures with different surface morphologies and volume fractions are formed from the same phase mask (Figure 2 b,c,d). Figure 2 b was obtained at low exposure time and with a large amount of inhibitor. The inset shows the cross-sectional view of the structure.[29] 3D structures with higher volume fractions than Figure 2 b are formed under conditions that lead to higher cross-linking density (e.g. longer exposure time and less inhibitor, Figure 2 c). Interestingly, flower-shaped structures, which are difficult to obtain with other techniques, are generated reproducibly when lightly
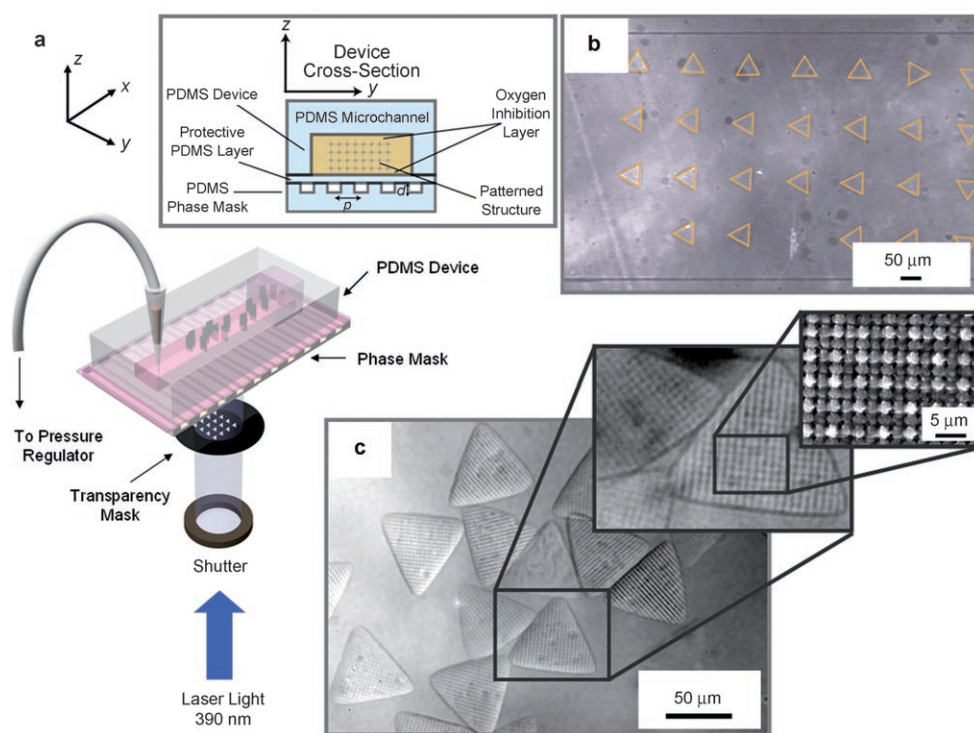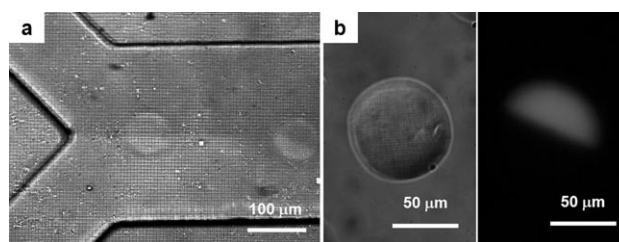

Figure 1. SFIL experimental setup. a) Schematic drawing showing the PDMS microfluidic device integrated with a PDMS phase mask. Shutter-regulated and transparency-mask-defined light from a pulsed laser or from a Hg lamp enters through the phase mask and into the stationary oligomer film that is contained in the microfluidic device. This procedure results in the formation of an array of structures, each of which contains a 3D pattern defined by the phase mask. The patterned particles are flushed out, and the flow is stopped before another array of particles is formed.[24] A cross-sectional view of the device is shown in the inset on the right side of (a). In our setup, the phase mask is separated from the liquid oligomer by a 3-μm-thick spin-coated layer of PDMS. The posts in the phase are arranged with $d = 1$ μm and $p = 2$ μm.
b) Brightfield image of an array of patterned triangles of side length 60 μm formed in a 600-μm-wide and 30-μm-tall microfluidic device. The triangles have been delineated because of the low contrast between the uncrosslinked oligomer and the particles. The granularity of the background is caused by the presence of the phase mask. c) DIC image of the triangles shown in (b) after they have been suspended in ethanol. The patterned grid-like structure formed by the phase mask is visible on the surface of the particles and seen more clearly in the inset SEM image.

Take advantage of blue reference links
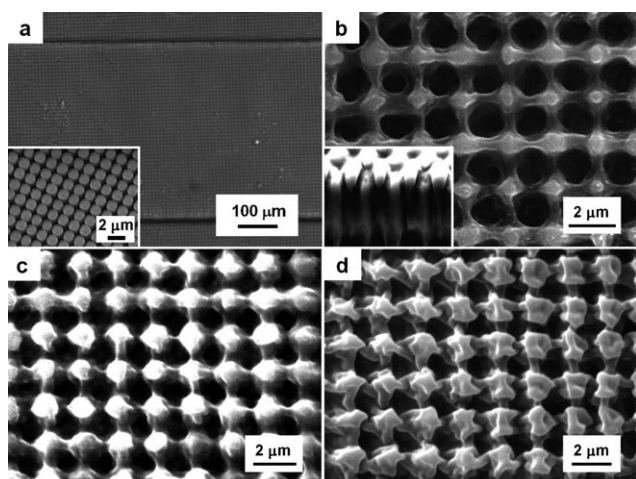
Figure 2. Images of PEGDA structures with various morphologies and volume fractions formed using the same phase mask. a) Optical microscopy image of the microfluidic channel viewed through the phase mask. The inset shows the SEM image of the phase mask. b) SEM image of a PEGDA structure fabricated in a microfluidic channel at short exposure time and with a large amount of inhibitor (700 ms, 1.2 wt% hydroquinone). The inset shows the cross-sectional view of the structure. c) SEM image of PEGDA fabricated at longer exposure time and with less inhibitor (1000 ms, 0.3 wt% hydroquinone). d) SEM image of a shrunken PEGDA structure with resultant flower shapes. Such structures are typically formed at much shorter exposure time than required to form firm posts (300 ms, 1.2 wt% hydroquinone).

Figure 3. Optical microscope images of Janus particles. a) DIC image of the microfluidic channel showing co-flow of rhodamine-labeled and unlabeled oligomer streams as well as faint images of circular prism regions after two stop-flow exposures. b) DIC image (left) and fluorescence microscopy image (right) of a three-dimensionally patterned Janus particle.

cross-linked hydrogel structures shrink in ethanol (Figure 2 d). The controlled porosity of such structures may be useful for applications such as size-based separations or to serve as flow-through stretching devices for DNA.

An important advantage of laminar flow in microfluidic devices is that it permits the creation of chemical anisotropy in flowing liquids. The flow can be homogenized only by the slow process of diffusive mixing, since convective mixing is negligible at these length scales. Several applications of this chemical confinement phenomenon have been reported, including the synthesis of chemically inhomogeneous particles.[22,25] One unique advantage of combining IL with microfluidics is the ability to synthesize chemically inhomogeneous 3D structures. As an illustrative example, Janus particles, which have two hemispheres made of different materials, with 3D patterns can be synthesized by co-flowing parallel streams of two different monomers (PEGDA and rhodamine-labeled PEDGA, Figure 3a). A brightfield image and a fluorescent image of a 75-µm-diameter circular disk, only half of which has been labeled with fluorescent dye, are shown in the left and right of Figure 3b, respectively. The anisotropy of the structures can be tuned by moving the position of the fluid–fluid interface relative to the light-intensity pattern. It is also possible to synthesize structures with concentration or porosity gradients using similar methods. In tissue engineering, such structures may be used to create a gradient of molecules on the surface of a biocompatible scaffold or to localize growth factors in a specific region. These factors can influence cell adhesion and migration, thus providing functional cues to cells.[2]

One of the most promising uses of polymeric particles is for sensing and diagnostic applications.[3] In such applications, a probe molecule on the surface of the particle binds to a target fluorophore molecule in solution. The particles are then washed to remove unbound fluorescent target molecules. The presence of the target in the original solution can be inferred from the intensity of the fluorescent signal emanating from the particle surface. The sensitivity of such particle-detection assays is critically dependent on the number of probe molecules that are present on the surface of the particle. Increasing the surface area of the particles by creating intricate patterned networks on the surface enables the synthesis of particles with extremely high ratios of surface area to volume. We formed 500-µm-diameter, 50-µm-tall disk-shaped hydrogel particles containing probe DNA molecules (Figure 4) using SFIL. These particles were then mixed with target DNA fluorophore molecules for hybridization and subsequently washed to remove unbound target. We find that the use of SFIL permits a tenfold increase in signal intensity compared to that observed with the control structure, which was a flat hydrogel structure formed without IL. When there is a great excess of target molecules compared to probe molecules, light intensity is assumed to vary linearly with probe density. Therefore, the surface area of the SFIL structures is inferred to be an order of magnitude greater than that of the control structures. This result implies that biosensors with 3D patterns could be used to greatly increase the sensitivities in particle assays.

In conclusion, we have shown that combining interference lithography with a flow-through microfluidic device offers several advantages. By synthesizing structures in hydrogel polymers that are not usually amenable to spin-coating, we are able to expand the range of materials available to interference lithography. The use of SFIL permits the high-throughput synthesis of mask-defined 3D structures whose length scales span three orders of magnitude (e.g. 1–1000 µm). In addition, various 3D structures with different surface areas and morphologies could be generated from one phase mask by controlling the interference intensity distribution of light and the concentration of inhibitor. By adopting a stop-flow exposure scheme, particles with 3D structures at the sub-micrometer scale were generated in a high-throughput
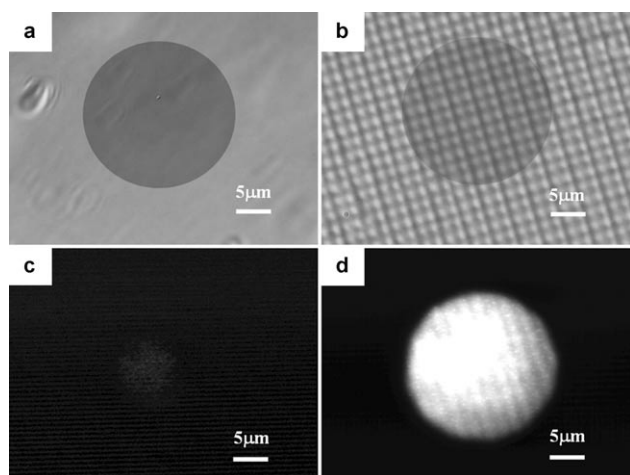
Figure 4. Increased detection sensitivity provided by patterned structures over unpatterned structures. a) Brightfield optical image of a flat hydrogel structure formed without IL. b) Brightfield image of a patterned structure formed using SFIL. c) Image of the region highlighted in (a) taken using a fluorescence microscope. The signal shown is very weak because of the low density of probe molecules on the surface of the particles. d) Fluorescent image of the structure seen in (b). The signal shown is strong at the same conditions as in (c) because of the high density of probe molecules on the surface. In (c) and (d), the field-stop aperture was closed down to collect signal from a small circular portion of the structure, corresponding to the highlighted regions in (a) and (b), respectively.

fashion in a microfluidic device. A wide range of materials, such as stimuli-responsive polymers, biocompatible polymers, and polymer–nanoparticle composites, can also be used for particle structure formation. By exploiting the diffusion-limited mixing seen in a microfluidic device, we have synthesized chemically anisotropic 3D structures. Such structures may be used to provide optimal conditions for cell growth and viability in tissue-engineering applications. It was also shown that the high ratio of surface area to volume of the structures may be used to generate high fluorescent signal intensities that could be of benefit to a variety of sensing and diagnostic applications. SFIL could be used for the high-throughput generation of three-dimensionally patterned 2D structures to conduct cell-material assays in a multiplexed fashion or to fabricate large numbers of microtissue templates.[30] Optimizing the materials used could also result in the formation of sub-micrometer 3D colloidal particles by disconnecting the structures after formation.[31]

Experimental Section
Details of the fabrication of the PDMS phase mask, the microfluidic device, and the stop-flow lithography setup are given in the Supporting Information.

Photopolymerization setup: A 100 W HBO mercury lamp with an i-line filter (Omega Optical) was used to provide 365.5-nm UV light. Light was collimated by passing the unfocused light (no objective in place) from the microscope through a 30-cm-long, 1-cm-diameter hollow metallic tube that was blackened on the inside. Light intensity was measured to be 5 mWcm^{-2}. A VS25 shutter system (Uniblitz) driven by a computer-controlled VMM-D1 shutter driver provided specified doses of UV light. Typical exposure times used

were 500–1000 ms. If required, photo masks (CAD Art Services, Bandor, OR) were inserted into the field stop of the microscope.

Photopolymerization: The 3D structures were made using 1 wt% Irgacure 819 (Sigma Aldrich) or Irgacure 184 initiator and 0.6–1.2 wt% hydroquinone in poly(ethylene glycol) (400) diacrylate (PEGDA, Polysciences). Exposure for 300–1000 ms with pulses of 160 fs from the frequency-doubled output of a Ti:sapphire laser operating at 390 nm and a repetition rate of 250 kHz were used. The sample morphology was analyzed with SEM (JEOL 6060 and FESEM JSM-7401)

Oligonucleotide incorporation: For hybridization experiments, we used monomer solutions of 2:1 PEGDA:TE Buffer [10 mM 2-amino-2-hydroxymethyl-1,3-propanediol (Tris) pH 8.0 (Rockland), 1M minocycline/ethylenediaminetetraacetic acid (MEDTA, Omni-Pur)] with 1% initiator and a DNA oligomer probe at a concentration of 50 μM. Oligomer probes (IDT) came modified with a reactive acrydite group and 18-carbon spacer (Probe #1: 5 Acrydite-C18ATA GCA GAT CAG CAG CCA GA-3, probe #2: 5 Acrydite-C18CAC TAT GCG CAG GTT CTC AT-3).

Oligonucleotide detection: Particles were pipetted into separate PDMS reservoirs for each hybridization experiment. Complementary target DNA oligomers modified with a Cy3 fluorophore (IDT) were suspended at a concentration of 1 μM in hybridization buffer [TE buffer with 0.2 M NaCl (Mallinckrodt) and 0.5% sodium dodecyl sulfate (SDS, Invitrogen)]. Solutions of target oligomer were pipetted into the appropriate reservoirs, and the particles were incubated for 10 min at room temperature. The particles were then rinsed several times with TE buffer and visualized using an orange longpass filter set (XF101–2, Omega), which is compatible with both rhodamine B and Cy3 fluorophores. Still images were captured using a Nikon D200 digital camera.

[1] R. S. Kane, S. Takayama, E. Ostuni, D. E. Ingber, G. M. Whitesides, *Biomaterials* **1999**, *20*, 2363.
[2] A. Khademhosseini, R. Langer, J. Borenstein, J. P. Vacanti, *Proc. Natl. Acad. Sci. USA* **2006**, *103*, 2480.
[3] D. C. Pregibon, M. Toner, P. S. Doyle, *Science* **2007**, *315*, 1393.
[4] Y. Lu, Y. D. Yin, Y. N. Xia, *Adv. Mater.* **2001**, *13*, 415.
[5] D. A. Parthenopoulos, P. M. Rentzepis, *Science* **1989**, *245*, 843.
[6] C. J. Bettinger, E. J. Weinberg, K. M. Kulig, J. P. Vacanti, Y. D. Wang, J. T. Borenstein, R. Langer, *Adv. Mater.* **2006**, *18*, 165.
[7] F. Gelain, D. Bottai, A. Vescovi, S. Zhang, *PLoS ONE* **2006**, *1*, e119.
[8] E. L. Thomas, D. B. Alward, D. J. Kinning, D. C. Martin, D. L. Handlin, L. J. Fetters, *Macromolecules* **1986**, *19*, 2197.
[9] S. Zhang, *Proc. Natl. Acad. Sci. USA* **2003**, *21*, 1171.
[10] A. D. Dinsmore, A. G. Yodh, D. J. Pine, *Phys. Rev. E* **1995**, *52*, 4045.
[11] J. C. Galas, B. Belier, A. Aassime, J. Palomo, D. Bouville, J. Aubert, *J. Vac. Sci. Technol. B* **2004**, *22*, 1160.
[12] G. M. Gratson, M. J. Xu, J. A. Lewis, *Nature* **2004**, *428*, 386.
[13] S. Kawata, H. B. Sun, T. Tanaka, K. Takada, *Nature* **2001**, *412*, 697.
[14] J. H. Jang, C. K. Ullal, M. Maldovan, T. Gorishnyy, S. E. Kooi, C. Koh, E. L. Thomas, *Adv. Funct. Mater.* **2007**, DOI: 10.1002/adfm.200700140.
[15] J. A. Rogers, K. E. Paul, R. J. Jackman, G. M. Whitesides, *J. Vac. Sci. Technol. B* **1998**, *16*, 59.
[16] J. H. Jang, C. K. Ullal, T. Gorishnyy, V. V. Tsukruk, E. L. Thomas, *Nano Lett.* **2006**, *6*, 740.

[17] S. Jeon, J. U. Park, R. Cirelli, S. Yang, C. E. Heitzman, P. V. Braun, P. J. A. Kenis, J. A. Rogers, *Proc. Natl. Acad. Sci. USA* **2004**, *101*, 12428.

[18] M. Campbell, D. N. Sharp, M. T. Harrison, R. G. Denning, A. J. Turberfield, *Nature* **2000**, *404*, 53.

[19] S. Yang, J. Ford, C. Ruengruglikit, Q. R. Huang, J. Aizenberg, *J. Mater. Chem.* **2005**, *15*, 4200.

[20] C. K. Ullal, M. Maldovan, E. L. Thomas, G. Chen, Y. J. Han, S. Yang, *Appl. Phys. Lett.* **2004**, *84*, 5434.

[21] S. C. Glotzer, M. J. Solomon, N. A. Kotov, *AIChE J.* **2004**, *50*, 2978.

[22] D. Dendukuri, D. C. Pregibon, J. Collins, T. A. Hatton, P. S. Doyle, *Nat. Mater.* **2006**, *5*, 365.

[23] J. W. Kim, A. S. Utada, A. Fernandez-Nieves, Z. B. Hu, D. A. Weitz, *Angew. Chem.* **2007**, *119*, 1851; *Angew. Chem. Int. Ed.* **2007**, *46*, 1819.

[24] D. Dendukuri, S. S. Gu, D. C. Pregibon, T. A. Hatton, P. S. Doyle, *Lab Chip* **2007**, *7*, 818.

[25] D. Dendukuri, T. A. Hatton, P. S. Doyle, *Langmuir* **2007**, *23*, 4669.

[26] C. Decker, A. D. Jenkins, *Macromolecules* **1985**, *18*, 1241.

[27] H. A. Stone, A. D. Stroock, A. Ajdari, *Annu. Rev. Fluid Mech.* **2004**, *36*, 381.

[28] S. Yang, M. Megens, J. Aizenberg, P. Wiltzius, P. M. Chaikin, W. B. Russel, *Chem. Mater.* **2002**, *14*, 2831.

[29] Since there is a residual nonzero background of the interference intensity, and the registry of the interference pattern occurs simultaneously with photocrosslinking, we find that the structures do not yet show fully open 3D pores throughout. Further optimization of the hydrogel materials and the phase mask should enable high-porosity hydrogel/air bicontinuous structures to be achieved.

[30] M. C. Cushing, K. S. Anseth, *Science* **2007**, *316*, 1133.

[31] J. H. Jang, C. K. Ullal, S. E. Kooi, C. Koh, E. L. Thomas, *Nano Lett.* **2007**, *7*, 647.

Take advantage of blue reference links